Supplementary Information

Industrial amine blends enable efficient CO electrosynthesis in reactive capture

Siyu Sonia Sun[1]†, Yurou Celine Xiao[1]†, Feng Li[1], Jinhong Wu[1], Yuxuan Che[1], Yong Wang[1], Min Liu[1], Yaohao Guo[1], Mengyang Fan[1], Kai Han[2], Paul-Emmanuel Just[2], Paul J. Corbett[2], Rui Kai Miao[1*], David Sinton[1*]

[1]*Department of Mechanical and Industrial Engineering, University of Toronto, Ontario, Canada*

[2]*Shell Global Solutions International B.V., Grasweg 31, 1031HW Amsterdam, the Netherlands*

**Corresponding author. Email: sinton@mie.utoronto.ca, ruikai.miao@mail.utoronto.ca*

†*These authors contributed equally to this work.*

COMSOL simulations

We simulated CO_2 distributions on the cathode surface in 1D with COMSOL Multiphysics package based on the finite-element-method solver. The HCO_3^- concentration was set to the range of 0.1 M to 1.8 M, simulating different amine blends as catholyte. The flux of H^+ was set on the membrane boundary according to the applied reaction current.

The concentrations of CO_2(aq), CO_3^{2-}, HCO_3^- and pH were calculated using the following homogeneous reactions:

$$CO_2 + H_2O \overset{k_{1f},\ k_{1r}}{\leftrightarrow} HCO_3^- + H^+ \quad (K_1) \tag{S1}$$

$$HCO_3^- \overset{k_{2f},\ k_{2r}}{\leftrightarrow} CO_3^{2-} + H^+ \quad (K_2) \tag{S2}$$

$$CO_2 + OH^- \overset{k_{3f},\ k_{3r}}{\leftrightarrow} HCO_3^- \quad (K_3) \tag{S3}$$

$$HCO_3^- + OH^- \overset{k_{4f},\ k_{4r}}{\leftrightarrow} CO_3^{2-} + H_2O \quad (K_4) \tag{S4}$$

$$CO_2(aq) \overset{k_{5f}}{\rightarrow} CO_2(g) \quad (K_5) \tag{S5}$$

$$H_2O \overset{k_{wf},\ k_{wr}}{\leftrightarrow} H^+ + OH^- \quad (K_w) \tag{S6}$$

The following equations were the electrochemical reactions on the cathode surface:

$$CO_2(aq) + H_2O + 2e^- \rightleftarrows CO(g) + 2OH^- \tag{S7}$$

$$2H_2O + 2e^- \rightleftarrows H_2(g) + 2OH^- \tag{S8}$$

The rate of each species R_i was broken into carbonate equilibria as follows:

$$R_{CO_2} = \left(-[CO_2]_{aq}[H_2O]k_{1f} + [H^+][HCO_3^-]k_{1r}\right) + \left(-[CO_2]_{aq}[OH^-]k_{3f} + [HCO_3^-]k_{3r}\right) \tag{S9}$$

$$R_{CO_3^{2-}} = \left([HCO_3^-]k_{2f} - [H^+][CO_3^{2-}]k_{2r}\right) + \left([HCO_3^-][OH^-]k_{4f} - [H_2O][CO_3^{2-}]k_{4r}\right) \tag{S10}$$

$$R_{HCO_3^-} = \left([CO_2]_{aq}[H_2O]k_{1f} - [H^+]\left[HCO_3^-\right]k_{1r}\right) + \left(-\left[HCO\right.\right. \\ \left. + \left(-\left[HCO_3^-\right][OH^-]k_{4f} + [H_2O]\left[CO_3^{2-}\right]k_{4r}\right)\right. \quad \textbf{(S11)}$$

$$R_{H^+} = \left([CO_2]_{aq}[H_2O]k_{1f} - [H^+]\left[HCO_3^-\right]k_{1r}\right) + \left(\left[HCO_3^-\right.\right. \quad \textbf{(S12)}$$

$$R_{OH^-} = \left(-[CO_2]_{aq}[OH^-]k_{3f} + \left[HCO_3^-\right]k_{3r}\right) + \left(-\left[HCO_3^-\right.\right. \quad \textbf{(S13)}$$

The phase transform rates from aqueous CO_2 to gaseous CO_2 ($R_{PT,CO2}$) were calculated via:

$$R_{PT,CO_2} = K_6^f\left(C_{CO_2}^0 - C_{CO_2(aq)}^f\right) if\ C_{CO_2}^0 < C_{CO_2(aq)}^0 \quad \textbf{(S14)}$$

The values of the rate constants for reactions S1-S6 are given in **Supplementary Table 3**.

The CO_2 saturation concentration was calculated using Henry's law:

$$C_{CO_2,aq}^0 = K_H^0 C_{CO_2,g} \quad \textbf{(S15)}$$

where K_H^0 is Henry's constant and was given as a function of temperature T:

$$\ln K_H^0 = 93.2417 * \left(\frac{100}{T}\right) - 60.2409 + 23.3585 * \ln\left(\frac{T}{100}\right) \quad \textbf{(S16)}$$

where T was assumed to be 298.15 K in this study.

The saturated concentration of CO_2 in an electrolyte was giving by the following equation:

$$\log\left(\frac{C_{CO_2,aq}^0}{C_{CO_2,aq}}\right) = K_S C_S \quad \textbf{(S17)}$$

where C_S was the molar concentration of the electrolyte, and K_S was the Sechenov's constant that were calculated using the following equations:

$$K_S = \sum(h_{CO_2} + h_{ion}) \quad \textbf{(S18)}$$

$$h_{CO_2} = h^0_{CO_2} + h^T_{CO_2}(T - 298.15) \quad \textbf{(S19)}$$

Values of h for all species can be found in **Supplementary Table 4**.

Supplementary Table 1 | Diffusion coefficients in $m^2 s^{-1}$.

Constant	Value	References
D_{H^+}	9.311×10^{-9}	(1)
D_{K^+}	1.957×10^{-9}	(1)
D_{OH^-}	5.273×10^{-9}	(1)
D_{CO_2}	1.91×10^{-9}	(1)
$D_{HCO_3^-}$	1.185×10^{-9}	(1)
$D_{CO_3^{2-}}$	0.923×10^{-9}	(1)

Supplementary Table 2 | Solvation sizes in m.

Constant	Value	References
a_{H^+}	0.56×10^{-9}	(1)
a_{K^+}	0.662×10^{-9}	(1)
a_{OH^-}	0.6×10^{-9}	(1)
a_{CO_2}	0.23×10^{-9}	(1)
$a_{HCO_3^-}$	0.8×10^{-9}	(1)
$a_{CO_3^{2-}}$	0.788×10^{-9}	(1)

Supplementary Table 3 | Rate constants used for modelling.

Constant	Value	Units	References
k_{1f}	3.71×10^{-2}	s^{-1}	(1)
k_{1r}	1.99×10^{4}	s^{-1}	(1)
k_{2f}	59.99	s^{-1}	(1)

k_{2r}	2.28×10^{7}	$mol^{-1}m^{3}s^{-1}$	(1)
k_{3f}	2.23	$mol^{-1}m^{3}s^{-1}$	(1)
k_{3r}	5.23×10^{5}	s^{-1}	(1)
k_{4f}	6.0×10^{6}	$mol^{-1}m^{3}s^{-1}$	(1)
k_{4r}	1.07×10^{6}	s^{-1}	(1)
k_{5f}	2.29×10^{-1}	$mol\, m^{-3}s^{-1}$	(2)
k_{wf}	2.4×10^{-2}	$mol\, m^{3}s^{-1}$	(1)
k_{wr}	2.4×10^{6}	$mol^{-1}m^{3}s^{-1}$	(1)

Supplementary Table 4 | h parameters used to estimate Sechenov's constant in $m^{3}kmol^{-1}$.

Constant	Value	References
h_{K_+}	0.0922	(3)
h_{OH_-}	0.0839	(3)
h_{HCO3^-}	0.0967	(3)
$h_{CO3^{2-}}$	0.1423	(3)
$h_{CO_2}^{0}$	– 0.0172	(3)
$h_{CO_2}^{T}$	– 0.00038	(3)

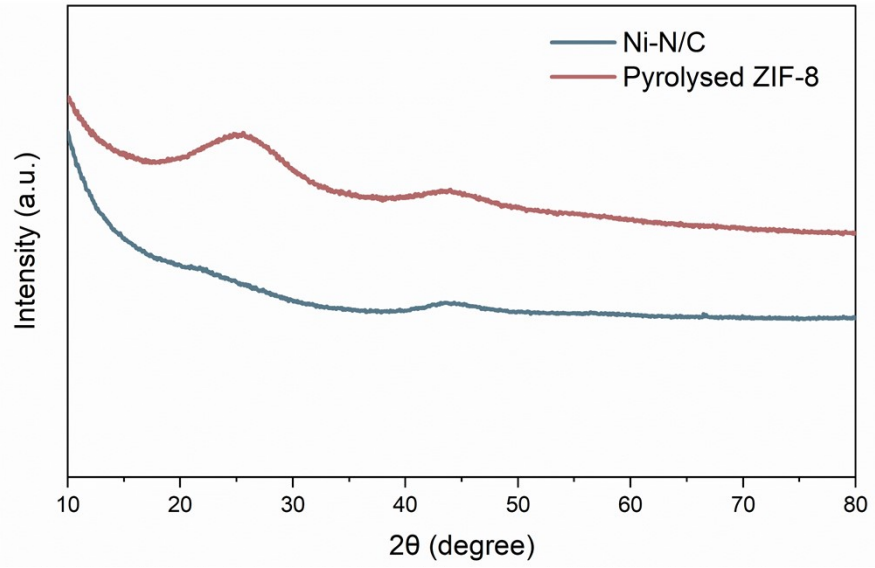

Supplementary Fig. 1 | XRD spectra of Ni-N/C and pyrolysed ZIF-8. The Ni-N/C powder sample showed no characteristic peaks associated with Ni or NiO(4). The two broad peaks observed in both powder samples were attributed to carbon planes(5,6).

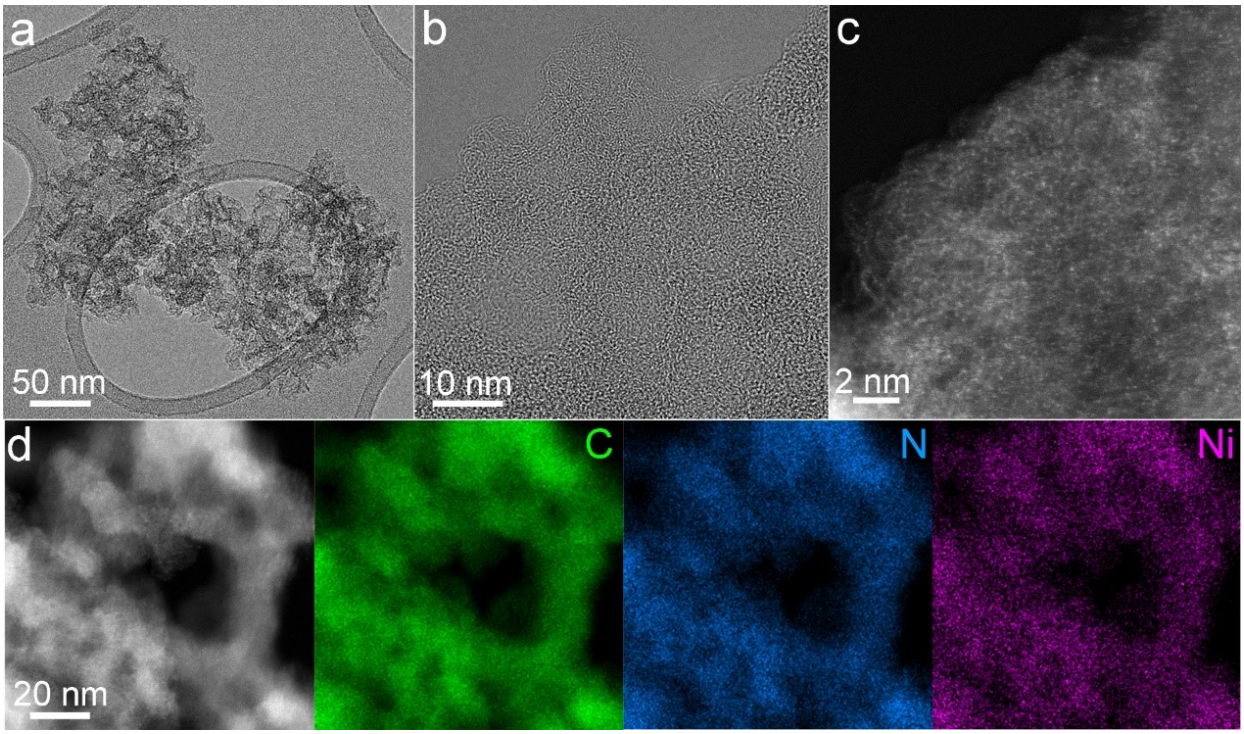

Supplementary Fig. 2 | Scanning transmission electron microscopy (STEM) images of the Ni-N/C catalyst. a – b, HRTEM images. **c,** high-magnification HAADF-STEM image of the Ni-N-C catalyst. **d,** HAADF-STEM image of the Ni-N-C catalyst and corresponding EDS elemental mappings of C, N, and Ni.

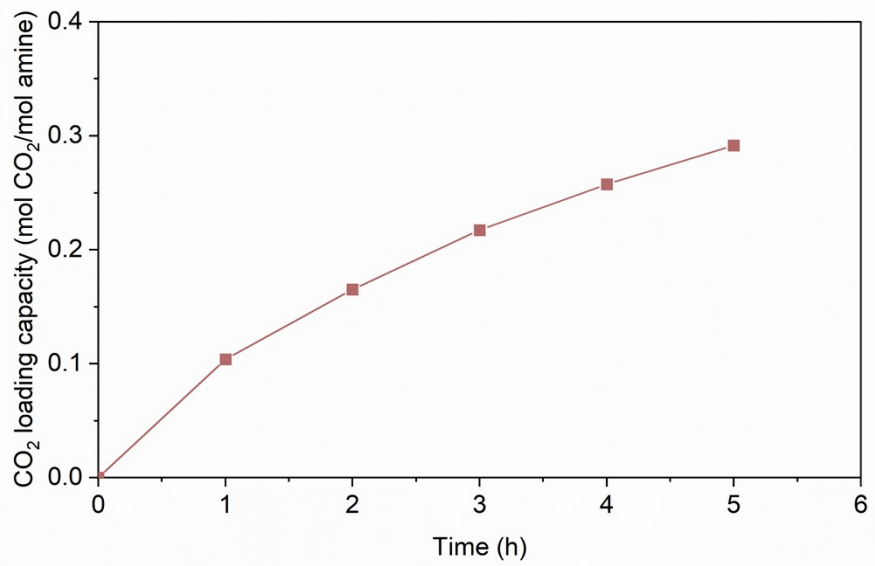

Supplementary Fig. 3 | Change in CO_2 loading over time during CO_2 absorption of 5 M MDEA.

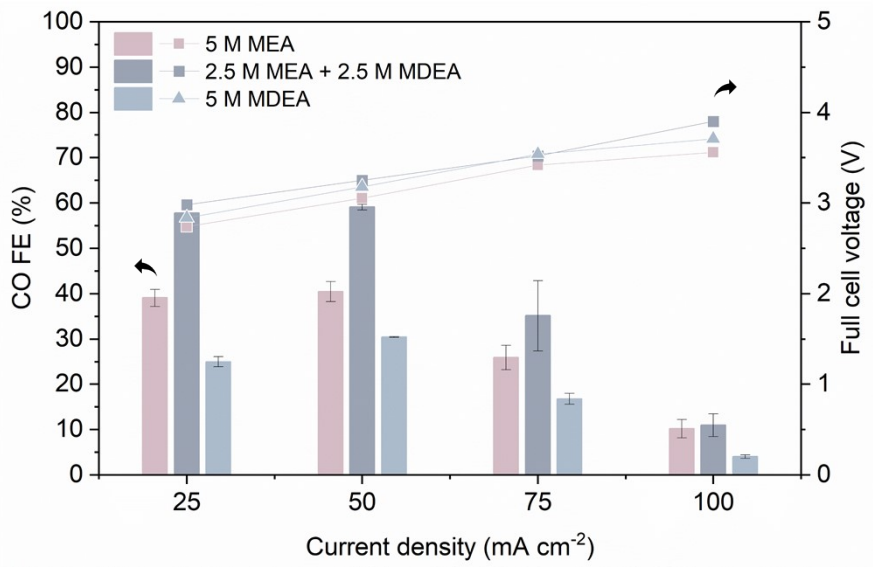

Supplementary Fig. 4 | FE towards CO and full cell voltage of 5 M MEA, 2.5 M MEA + 2.5 M MDEA, and 5 M MDEA solutions at the CO_2 loadings of 0.56 mol CO_2/mol amine, 0.56 mol CO_2/mol amine, and 0.29 mol CO_2/mol amine, respectively.

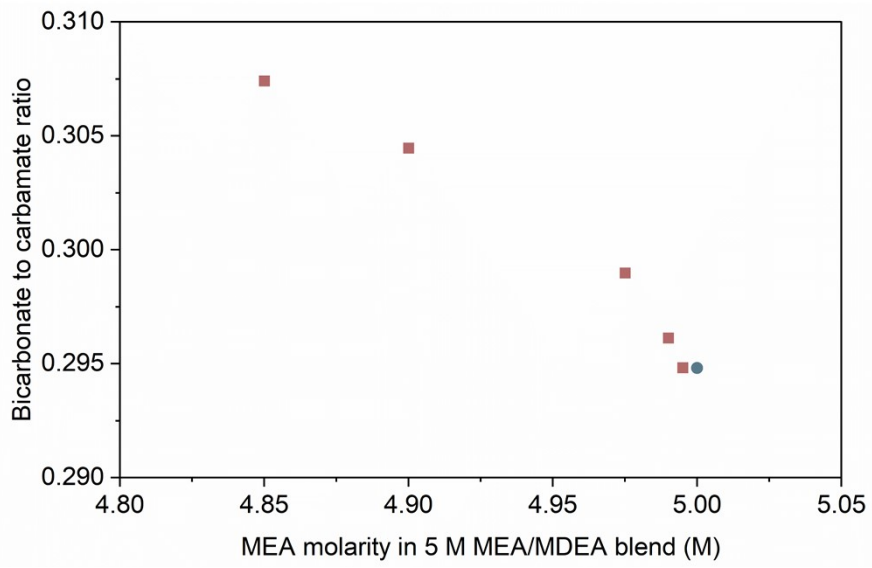

Supplementary Fig. 5 | Comparison of the bicarbonate-to-carbamate ratio for 5 M MEA and several 5 M MEA/MDEA blends.

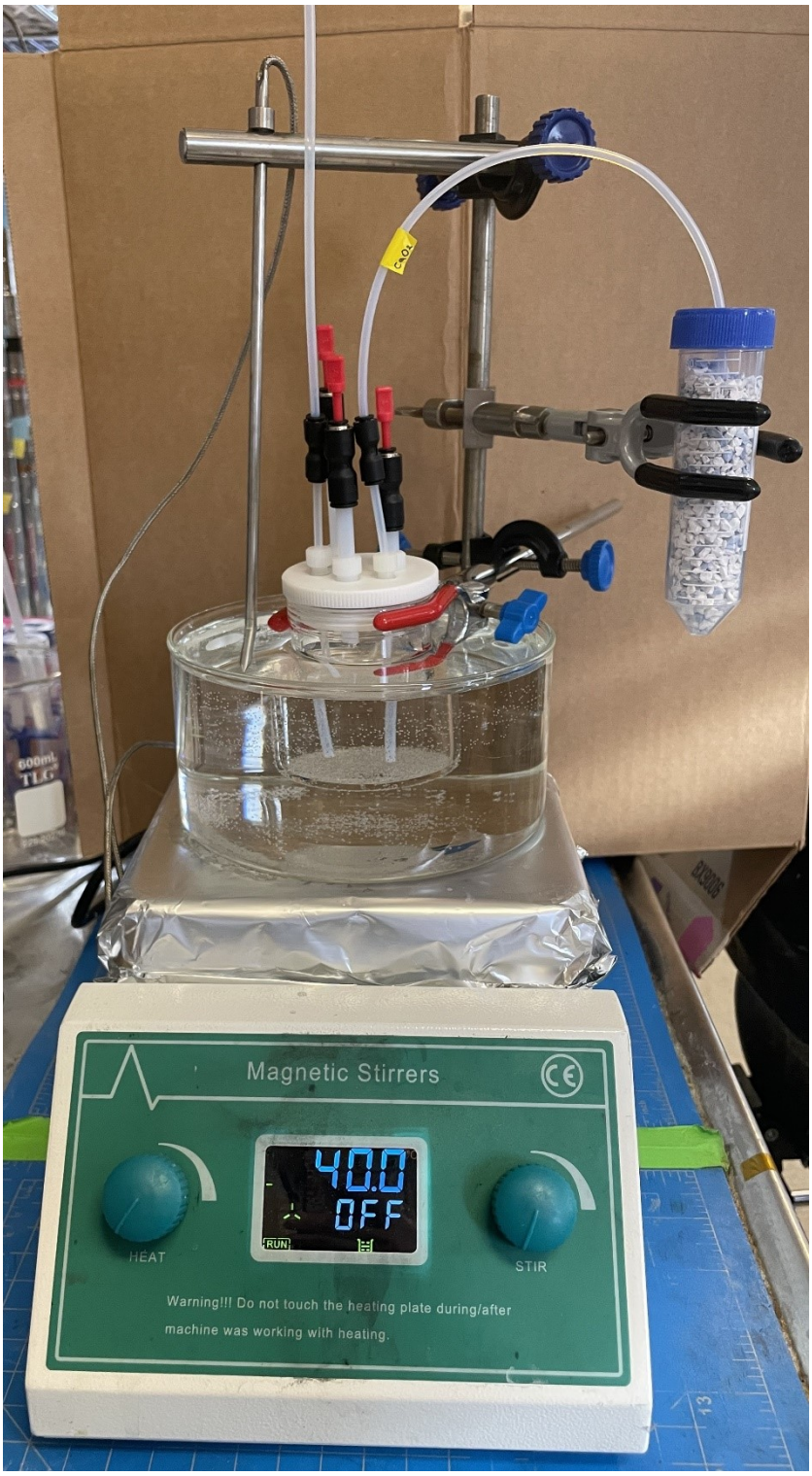

Supplementary Fig. 6 | Experimental setup for amine-based CO_2 capture under industrial absorption conditions.

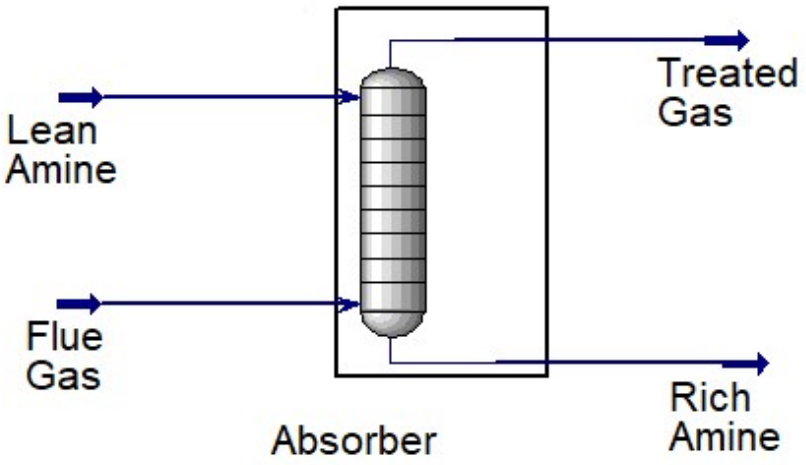

Supplementary Fig. 7 | Aspen HYSYS model for amine-based CO_2 capture under industrial absorption conditions.

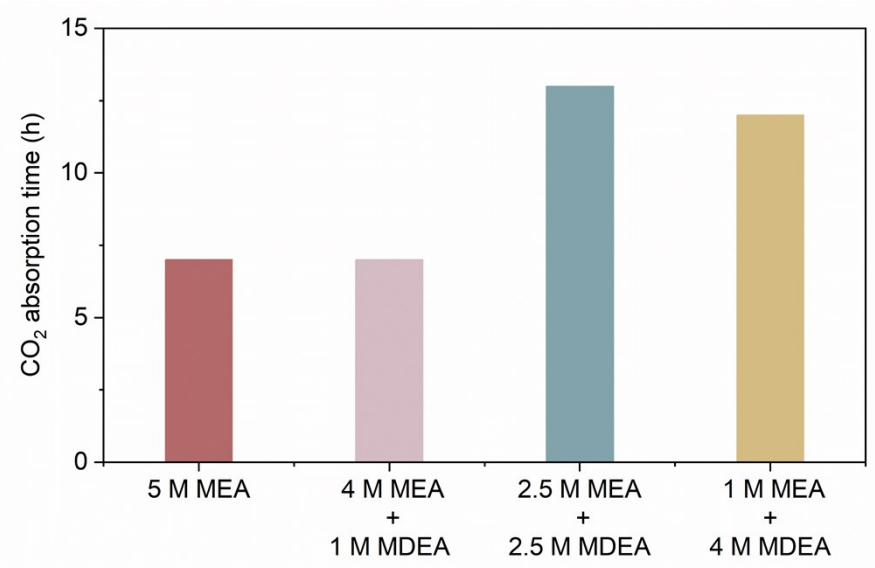

Supplementary Fig. 8 | Absorption time to reach respective CO_2 loading capacity purging with flue gas stream (15 vol% CO_2 in N_2) at 40 °C and 1 atm.

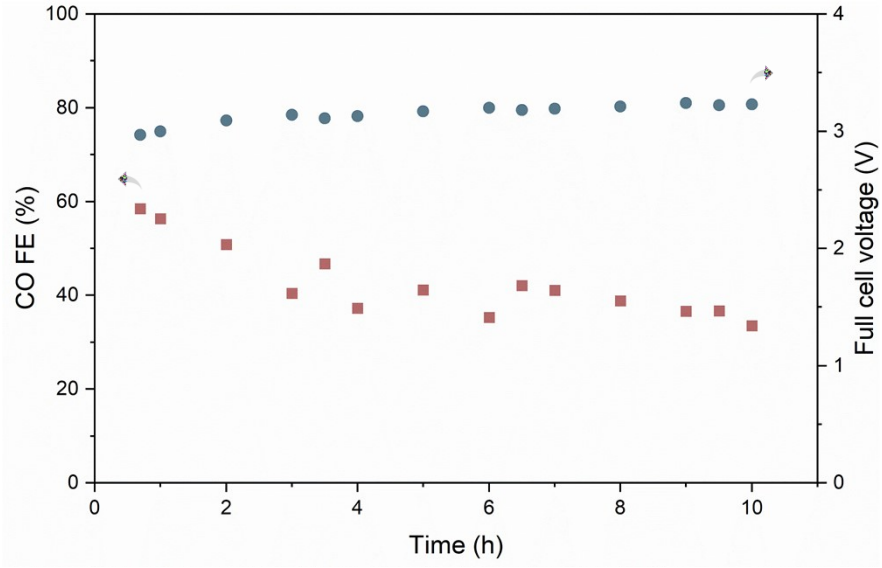

Supplementary Fig. 9 | Stability test with 4 M MEA + 1 M MDEA solution at its saturated CO_2 loading purged at room temperature and with 100 vol% CO_2 at atmospheric pressure, and electrolytes replaced every 3 h.

Supplementary Table 5 | Electrolyte conductivity of MEA/MDEA solutions and their series resistances during electrolysis measured using EIS.

	Conductivity (mS/m)	**Series Resistance, R_s (Ω)**
5 M MEA	30.5 ± 0.03	2.10 ± 0.01
4 M MEA + 1 M MDEA	21.4 ± 0.02	2.45 ± 0.01
2.5 M MEA + 2.5 M MDEA	11.84 ± 0.01	3.04 ± 0.01
1 M MEA + 4 M MDEA	5.21 ± 0.01	4.05 ± 0.01

Supplementary Table 6 | Comparison of the electrochemical performance with amine-based reactive CO_2 capture reports.

Capture solution	CO FE (%)	Current density (mA cm^{-2})	j_{CO} (mA cm^{-2})	Cathode potential (-V vs. RHE)	Full cell potential (V)	CO EE (%)	Ref.
2 M potassium glycinate (K-GLY) + 0.1 M monopotassium phosphate (KH_2PO_4)	44	200	89		3.2	19[a]	(7)
	64	50	32		2.7	31[a]	
5 M MEA	65	50	32				(8)
	78	2.6	2	0.63			
3 M triethylamine (TREA)	35	100	35		3.5	13	(9)
	70	20	14				
1 M 2-amino-2-methyl-1-propanol (AMP) + cetrimonium bromide (CTAB)	91	11	10	0.91			(10)
1 M AMP in polycarbonate (PC)	45	15	7	1.6			(11)
5 M MEA + 2 M potassium chloride (KCl)	72	50	36	0.8			(12)
0.4 M MDEA-based deep eutectic solvent (DES)	71	20	14	1.1			(13)
Ethylenediamine (EDA)	58	18.4	11	0.78			(14)
1.25 M 1-cyclohexylpiperidine (CHP)	26	104	27		4.2	8	(15)

	39	10	4	2.0	25	
3 M Piperazine	75	50	38	2.3	44[b]	(16)
	31	100	31	2.2	19[b]	

a. These electrolysis experiments were performed at 40 °C.

b. These electrolysis experiments were performed at 60 °C.

References

1. Bohra D, Chaudhry JH, Burdyny T, Pidko EA, Smith WA. Modeling the electrical double layer to understand the reaction environment in a CO_2 electrocatalytic system. Energy Environ Sci [Internet]. 2019 Oct 1 [cited 2025 Aug 28];12(11):3380–9. Available from: http://dx.doi.org/10.1039/C9EE02485A

2. Schulz KG, Riebesell U, Rost B, Thoms S, Zeebe RE. Determination of the rate constants for the carbon dioxide to bicarbonate inter-conversion in pH-buffered seawater systems. Mar Chem [Internet]. 2006 Jun 1 [cited 2025 Aug 28];100(1–2):53–65. Available from: https://www.sciencedirect.com/science/article/pii/S0304420305001684

3. Weisenberger S, Schumpe A. Estimation of gas solubilities in salt solutions at temperatures from 273 K to 363 K. AIChE J [Internet]. 1996 Jan [cited 2025 Aug 28];42(1):298–300. Available from: https://aiche.onlinelibrary.wiley.com/doi/10.1002/aic.690420130

4. Richardson JT, Scates R, Twigg M V. X-ray diffraction study of nickel oxide reduction by hydrogen. Appl Catal A Gen [Internet]. 2003 Jun 25 [cited 2025 Aug 28];246(1):137–50. Available from: https://www.sciencedirect.com/science/article/pii/S0926860X02006695

5. Liu W, Chen Y, Haifeng Q, Zhang L, Yan W, Liu X, et al. A durable nickel single-atom catalyst for hydrogenation reactions and cellulose valorization under harsh conditions. Angewandte Chemie [Internet]. 2018 Jun 11 [cited 2025 Aug 28];57(24):7071–5. Available from: https://onlinelibrary.wiley.com/doi/abs/10.1002/anie.201802231

6. Yang H, Shang L, Zhang Q, Shi R, Waterhouse GIN, Gu L, et al. A universal ligand mediated method for large scale synthesis of transition metal single atom catalysts. Nat Commun [Internet]. 2019 Oct 8 [cited 2025 Aug 28];10(1):4585. Available from: https://doi.org/10.1038/s41467-019-12510-0

7. Xiao YC, Sun SS, Zhao Y, Miao RK, Fan M, Lee G, et al. Reactive capture of CO_2 via amino acid. Nat Commun [Internet]. 2024 Sep 8 [cited 2025 Aug 28];15:7849. Available from: https://doi.org/10.1038/s41467-024-51908-3

8. Kim JH, Jang H, Bak G, Choi W, Yun H, Lee E, et al. The insensitive cation effect on a single atom Ni catalyst allows selective electrochemical conversion of captured CO_2 in universal media. Energy Environ Sci [Internet]. 2022 Aug 22 [cited 2025 Aug 28];15(10):4301–12. Available from: https://pubs.rsc.org/en/content/articlelanding/2022/ee/d2ee01825j

9. Langie KMG, Tak K, Kim C, Lee HW, Park K, Kim D, et al. Toward economical application of carbon capture and utilization technology with near-zero carbon emission. Nat Commun [Internet]. 2022 Dec 5 [cited 2025 Aug 28];13:7482. Available from: https://doi.org/10.1038/s41467-022-35239-9

10. Ahmad N, Chen Y, Wang X, Sun P, Bao Y, Xu X. Highly efficient electrochemical upgrade of CO_2 to CO using AMP capture solution as electrolyte. Renew Energy [Internet]. 2022 Apr [cited 2025 Aug 28];189:444–53. Available from: https://www.sciencedirect.com/science/article/pii/S0960148122002804

11. Pérez-Gallent E, Vankani C, Sánchez-Martínez C, Anastasopol A, Goetheer E. Integrating CO_2 capture with electrochemical conversion using amine-based capture solvents as electrolytes. Ind Eng Chem Res [Internet]. 2021 Mar 10 [cited 2025 Aug 28];60(11):4269–78. Available from: https://doi.org/10.1021/acs.iecr.0c05848

12. Lee G, Li YC, Kim JY, Peng T, Nam DH, Sedighian Rasouli A, et al. Electrochemical upgrade of CO_2 from amine capture solution. Nat Energy [Internet]. 2020 Dec 7 [cited 2025 Aug 28];6:46–53. Available from: https://www.nature.com/articles/s41560-020-00735-z#author-information

13. Ahmad N, Wang X, Sun P, Chen Y, Rehman F, Xu J, et al. Electrochemical CO_2 reduction to CO facilitated by MDEA-based deep eutectic solvent in aqueous solution. Renew Energy [Internet]. 2021 Nov [cited 2025 Aug 28];177:23–33. Available from: https://www.sciencedirect.com/science/article/pii/S0960148121007898

14. Abdinejad M, Mirza Z, Zhang X an, Kraatz H. Enhanced electrocatalytic activity of primary amines for CO_2 reduction using copper electrodes in aqueous solution. ACS Sustain Chem Eng [Internet]. 2020 Jan 15 [cited 2025 Aug 28];8(4):1715–20. Available from: https://doi.org/10.1021/acssuschemeng.9b06837

15. Diaz LA, Gao N, Adhikari B, Lister TE, Dufek EJ, Wilson AD. Electrochemical production of syngas from CO_2 captured in switchable polarity solvents. Green Chem [Internet]. 2017 Dec 14 [cited 2025 Aug 28];20(3):620–6. Available from: http://dx.doi.org/10.1039/C7GC03069J

16. Li P, Mao Y, Shin H, Yang Q, Cheng X, Li Y, et al. Tandem amine scrubbing and CO_2 electrolysis via direct piperazine carbamate reduction. Nat Energy [Internet]. 2025 Sep 11 [cited 2025 Aug 28];10:1262–73. Available from: https://doi.org/10.1038/s41560-025-01869-8